CrossMark

Synthesis of GO–AgIO$_4$ nanocomposites with enhanced photocatalytic efficiency in the degradation of organic pollutants

Zhenyuan Ji[1], Longhai Feng[1], Lirong Kong[1], Xiaoping Shen[1,*], Jiheng Wang[2], Keqiang Xu[1], and Xiaoyang Yue[1]

[1] *School of Chemistry and Chemical Engineering, Jiangsu University, Zhenjiang 212013, People's Republic of China*
[2] *School of Material Science and Engineering, Jiangsu University of Science and Technology, Zhenjiang 212003, People's Republic of China*

ABSTRACT

Graphene oxide (GO)–AgIO$_4$ nanocomposites with excellent photocatalytic performance have been prepared through a facile ion-exchange method. The as-prepared samples are characterized by X-ray diffraction, Fourier transform infrared spectroscopy, scanning electron microscopy, and transmission electron microscopy. The GO–AgIO$_4$ nanocomposites exhibit an enhanced photocatalytic activity in the degradation of organic pollutants as compared to bare AgIO$_4$. It is revealed that the introduction of GO can relieve the agglomeration of AgIO$_4$ particles, enhance the light absorption of the materials, and promote the separation of photoexcited electron–hole pairs. In addition, the possible transfer and separation behaviors of the charge carriers and the photocatalytic mechanism are discussed in detail. The excellent photocatalytic performance makes the GO–AgIO$_4$ nanocomposites a promising photocatalyst for organic pollutant treatment.

Introduction

Advanced oxidation processes, including Fenton [1–3] and photocatalytic oxidation [4], have been considered as promising treatment technologies for organic pollution removal because of their high removal efficiency than conventional methods. Among them, semiconductor photocatalysis was found to be prominent and practicable method for clean, economical, and environmentally friendly treatment of various organic pollutants by using solar energy [5–7]. Unfortunately, the most widely utilized photocatalyst of TiO$_2$ is only active under UV irradiation [8]. Therefore, exploiting novel and efficient photocatalysts that can work under visible light is necessary for practical wastewater treatment. Plenty of efforts have been made to explore efficient visible-light-driven catalysts for the degradation of organic pollutants [9, 10]. However, the low photocatalytic activity and poor stability of these photocatalysts are the main problems that limit their practical application [11–13]. Therefore, it is still a challenge to

develop new visible-light-driven photocatalysts with high photocatalytic activity and stability.

In recent years, graphene has been used as an ideal supporting material for photocatalysts due to its extraordinary properties such as super high surface area and excellent electron mobility [14–16]. A variety of graphene-based composite photocatalysts such as Ag_2CO_3–graphene [17, 18], Ag_3PO_4–graphene [19–21], AgX–graphene (X=Br, Cl), etc., have been reported [22–26]. These investigations found that graphene-based composite photocatalysts exhibit an enhanced photocatalytic performance in the degradation of organic pollutants as compared to their individual components. Thus, the preparation of graphene-based composite photocatalysts is a promising way to obtain high-efficient photocatalytic materials. Recently, Tang et al. [27] reported a novel $AgIO_4$ photocatalyst with excellent photocatalytic activity. However, the graphene-based $AgIO_4$ composite photocatalysts have not been reported so far. It is possible to further enhance the photocatalytic activity of $AgIO_4$ by combining it with graphene.

Herein, we report an effective ion-exchange method to synthesize the composites of $AgIO_4$ and graphene oxide (GO). The as-synthesized GO–$AgIO_4$ nanocomposites exhibit enhanced photocatalytic performances compared to bare $AgIO_4$ photocatalysts under simulated solar light (SSL) irradiation. In addition, the possible transfer and separation behaviors of the charge carriers and the photocatalytic mechanism are discussed in detail.

Experimental section

Materials

Natural flake graphite with a particle size of 150 μm (99.9% purity) was purchased from Qingdao Guyu Graphite Co., Ltd. All of the other chemical reagents employed in this study were obtained from Sinopharm Chemical Reagent Co., Ltd, which are of analytical grade and used as received without further purification. Graphite oxide was synthesized by a modified Hummers method [28, 29].

Synthesis of the photocatalysts

In a typical synthesis, a certain amount of graphite oxide was dispersed in 20 mL of distilled water by ultrasonication to give a GO dispersion. Then,

2 mmol of $AgNO_3$ dissolved in 10 mL of distilled water was added into the GO dispersion. After the mixture was vigorously stirred for 2 h, 10 mL of Na_2MoO_4 (1 mmol) aqueous solution was dropwise added into the above mixture under stirring. After reacting for 30 min, 4 mmol of HIO_4 was added and the resulted mixture was stirred for 1 h. The GO–$AgIO_4$ product was collected by centrifugation, washed with water and absolute ethanol, respectively, and then dried at 45 °C in a vacuum oven. The synthetic process of GO–$AgIO_4$ nanocomposites is illustrated in Fig. 1. To investigate the effect of the amount of GO on the photocatalytic activity of GO–$AgIO_4$ composites, the GO–$AgIO_4$ nanocomposites with GO contents of 0, 2, 7, and 10 wt% were prepared and denoted as $AgIO_4$, 2%GO–$AgIO_4$, 7%GO–$AgIO_4$, and 10%GO–$AgIO_4$, respectively. For comparison, the sample of $AgIO_4$ (Ref) was prepared by the direct reaction of $AgNO_3$ with HIO_4 according to the method reported in literature [27]. In addition, partially reduced graphene oxide (pRGO)–$AgIO_4$ and RGO–$AgIO_4$ photocatalysts were also prepared according to the literature methods [30, 31].

Characterization

The phases of the as-obtained products were characterized by X-ray diffraction (XRD) on a Bruker D8 Advance diffractometer with Cu K_α radiation ($\lambda = 1.5406$ Å) at a scanning rate of 7° min^{-1}. The Raman spectra were acquired on a DXR Raman spectrometer with a 532 nm wavelength incident laser light at room temperature. The morphologies of
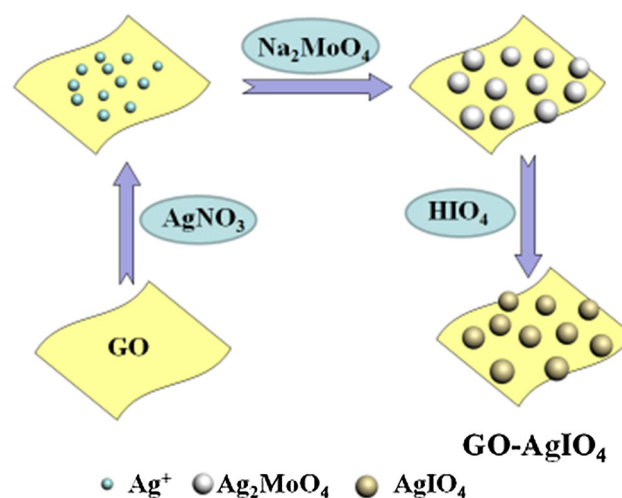

Figure 1 Synthesis process of GO–$AgIO_4$ nanocomposites.

the products were determined by scanning electron microscopy (SEM, JSM-6480) and transmission electron microscopy (TEM, JEOL JEM-2100). The loading amounts of $AgIO_4$ in the $GO/AgIO_4$ nanocomposites were examined by an inductively coupled plasma-optical emission spectrometer (ICP-OES, Vista-MXP, Varian). Fourier transform infrared (FT-IR) spectra were recorded on a Nicolet Nexus 470 spectrophotometer with KBr pellets in the 4000–400 cm^{-1} region. Ultraviolet–visible (UV–Vis) absorption spectra were recorded with a UV-1800PC UV–Vis spectrophotometer. UV–Vis diffuse reflectance spectra were conducted with a UV-2450 UV–Vis spectrophotometer. The photoluminescence properties of the samples were measured with a photoluminescence (PL) spectrometer (Varian Cary Eclipse).

Photocatalytic activity measurement

The photodegradation reaction was conducted in a GHX-3 photochemical reactor (Science and Education Equipment Co., Ltd, Yangzhou, China). A 250-W Xe lamp serving as the SSL source was positioned at ca.10 cm away from the reaction cell to trigger the photocatalytic reaction. The output wavelength spectrum of this lamp is shown in Fig. S1. There is a water layer between the reaction system and the lamp to remove the thermal effect of light. The photocatalytic activities of the samples were evaluated by the photocatalytic degradation of three different kinds of organic pollutants including methylene blue (MB), rhodamine B (RhB), and methyl orange (MO) under the SSL irradiation. Aqueous solutions (100 mL, 10 mg L^{-1}) of MB, RhB, and MO were, respectively, used in the photodegradation processes. In each experiment, 10 mg of photocatalyst was added into the pollutant solution. Before illumination, the suspension was stirred in the dark for 1 h to ensure the establishment of an adsorption–desorption equilibrium between the photocatalyst and the pollutant. All the experiments were performed at 25 °C under constant stirring. At regular time intervals, 4 mL of the suspension was taken out from the reaction vessel and pipetted into a centrifuge tube. After centrifuged at 12000 rpm for 3 min to separate the remnant photocatalyst from the solution, the supernatant was taken out to determine its concentration by measuring its absorbance with an UV–Vis spectrophotometer. The characteristic absorption wavelengths of MB, RhB, and MO were 664, 554, and 464 nm, respectively. The photodegradation ratio was calculated using the relative concentration (C/C_0) of the organic pollutants, where C_0 is the calculated concentration of the organic pollutant after adsorption equilibrium, and C is the residual concentration at different irradiation time. In the recycle experiments, the photocatalyst was separated from the solution, washed with ethanol and DI water, and then re-dispersed in the dye solution for another cycle.

Results and discussion

Characterization of the as-prepared photocatalysts

X-ray diffraction (XRD) is used to investigate the crystalline phases of the as-synthesized samples, and the corresponding XRD patterns are shown in Fig. 2. For the $AgIO_4$ sample, the peaks at 2θ of 18.1°, 29.6°, 33.3°, 38.1°, 47.9°, 56.2°, 61.3°, and 62.9° can be, respectively, indexed to (101), (004), (200), (211), (220), (312), (008), and (321) reflections of $AgIO_4$ (JCPDS No. 10-0368). No any peaks from impurities can be observed in the XRD pattern, indicating that the $AgIO_4$ sample is highly pure. It is interesting to note that the $AgIO_4$ (Ref) prepared by the direct reaction of $AgNO_3$ with HIO_4 possesses a quite different crystal structure [27], which cannot be indexed to the $AgIO_4$ standard card of JCPDS No. 10-0368. As usual, graphite oxide shows an intense diffraction peak at around 12°, corresponding to its (002) reflection [32]. The XRD pattern of 7%GO-$AgIO_4$ nanocomposite is similar to that of $AgIO_4$ sample, and no discernible diffraction peaks from graphite oxide are observed, which can be attributed to the low content of GO in these composites and/or the forestalled stack of GO sheets due to the attachment of inorganic units on them [33–35]. In addition, no observable shift in any of the $AgIO_4$ reflections after combination with GO. These findings demonstrate that $AgIO_4$ was not substituted into the position of oxide in GO, but rather presented as a discrete (predominantly) $AgIO_4$ phase dispersed on the GO surface [4]. Raman spectroscopy is a powerful and nondestructive technique to investigate the structure of carbon-based materials. Figure 2b shows the Raman spectra of as-prepared $AgIO_4$ and 7%GO–$AgIO_4$ nanocomposite. It can be seen that besides the
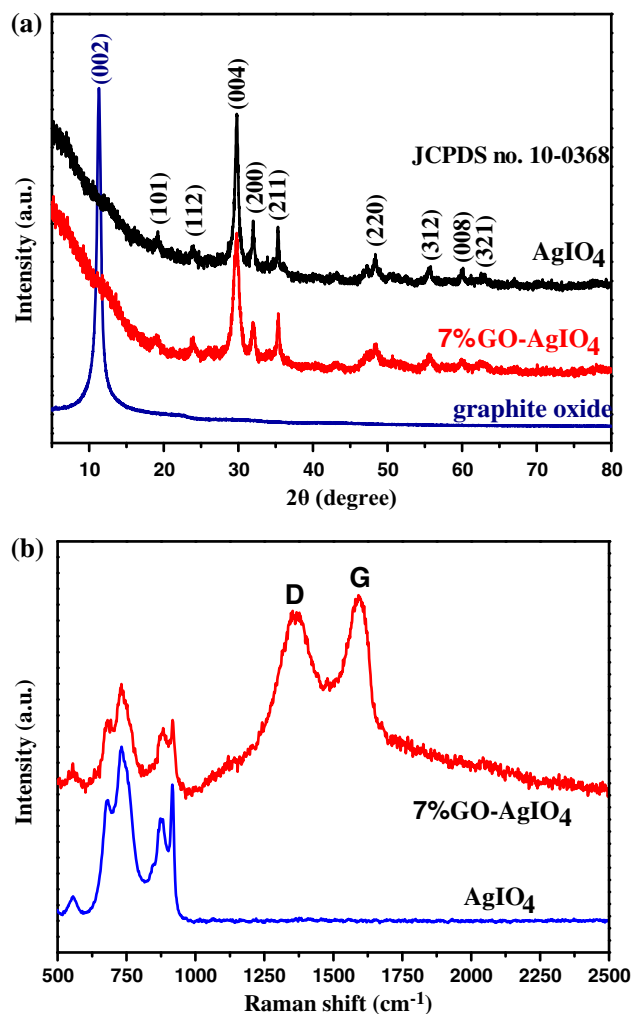
Figure 2 **a** XRD patterns of the obtained graphite oxide, $AgIO_4$ and 7%GO–$AgIO_4$ nanocomposite; **b** Raman spectra of $AgIO_4$ and 7%GO–$AgIO_4$ nanocomposite.

Figure 3 FT-IR spectra of the as-prepared graphite oxide, $AgIO_4$ and 7%GO–$AgIO_4$ nanocomposite.

peaks from $AgIO_4$, two prominent characteristic peaks can be observed in the Raman spectrum of 7%GO–$AgIO_4$ nanocomposite, which are attributed to the well-documented D and G bands of GO. This further confirms the formation of GO–$AgIO_4$ nanocomposite. Moreover, the $AgIO_4$ peaks in 7%GO–$AgIO_4$ show no appreciable shifts relative to those of pure $AgIO_4$, further indicating negligible $AgIO_4$ substitution into the position of oxide in GO.

FT-IR spectra were further used to analyze the compositions and structures of the as-synthesized samples. As shown in Fig. 3, in the FT-IR spectrum of graphite oxide, the broad band at 3250–3500 cm^{-1} is attributed to the stretching vibration of O–H groups [36], and the peak at 1375 cm^{-1} corresponds to the C–H bending [37]. In addition, the band corresponding
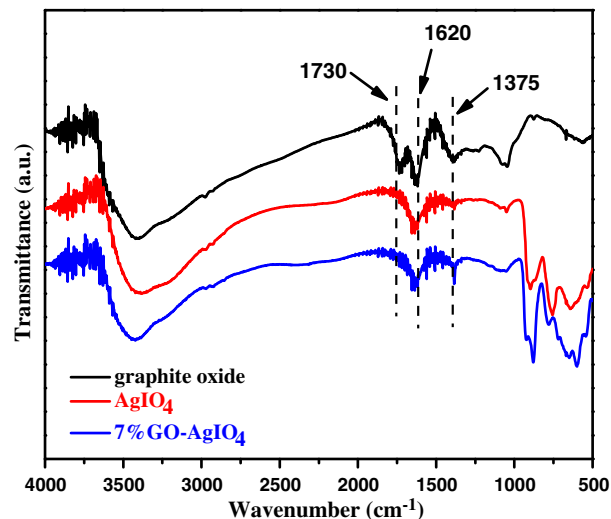
to C=O stretching of –COOH groups is at around 1730 cm^{-1} and the band corresponding to O–H bending vibration appears at 1620 cm^{-1} [38, 39]. In the IR spectrum of 7%GO–$AgIO_4$, except for the peaks from graphite oxide, other absorption peaks are similar to those of pure $AgIO_4$. This result implies that the GO–$AgIO_4$ nanocomposite has been successfully prepared.

The particle size and microstructure of the as-prepared $AgIO_4$ and GO–$AgIO_4$ nanocomposite were examined by SEM and TEM. Figure 4a, b shows the SEM image of pure $AgIO_4$. The $AgIO_4$ particles show big size and irregular morphology due to the severe agglomeration. As shown in the TEM images of GO–$AgIO_4$ nanocomposites (Fig. 4c and Fig. S2), the transparent GO nanosheets are fully coated by $AgIO_4$ particles, and $AgIO_4$ particles exclusively anchor on GO nanosheets, suggesting the good combination of $AgIO_4$ and GO. The mean particle sizes of the decorated $AgIO_4$ in 2%GO–$AgIO_4$, 7%GO–$AgIO_4$, and 10%GO–$AgIO_4$ nanocomposites are about 654, 514, and 353 nm, respectively. Notably, the diameter of the $AgIO_4$ particles becomes much smaller than the pure $AgIO_4$ particles. It is because GO nanosheets with large surface area can provide a great number of deposition sites for $AgIO_4$ particles and thus prevent their agglomeration [35]. In order to determine the exact compositions of GO–$AgIO_4$ nanocomposites, ICP-OES analysis was carried out. The GO contents in 2%GO–$AgIO_4$, 7%GO–$AgIO_4$, and 10%GO–$AgIO_4$
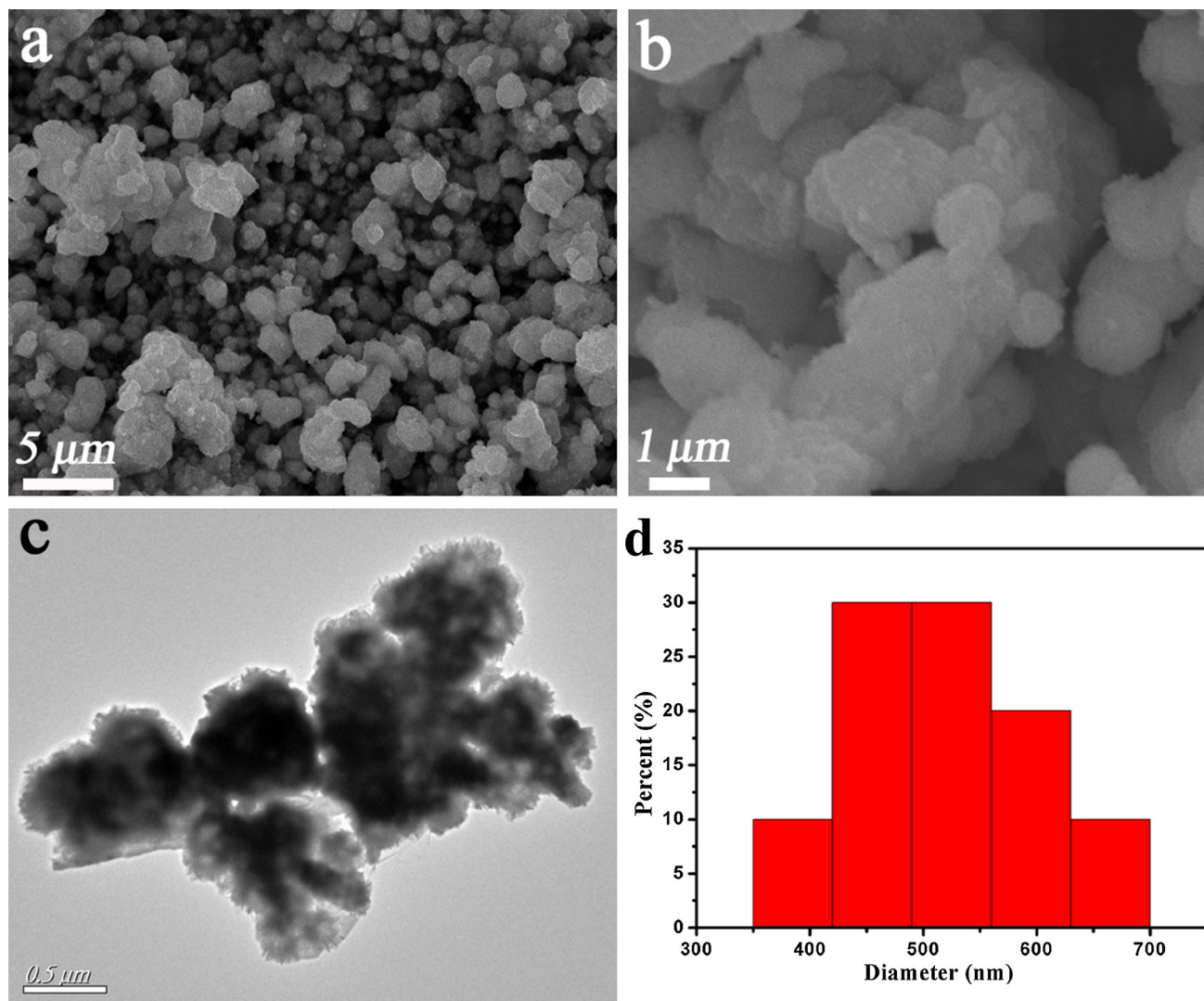
Figure 4 **a**, **b** SEM images of pure AgIO$_4$; **c** TEM image of 7%GO–AgIO$_4$ nanocomposite; **d** the size distribution of AgIO$_4$ nanoparticles in the nanocomposite.

nanocomposites were determined to be about 1.8, 6.6, and 9.5 wt%, respectively.

The optical absorption properties of the as-prepared photocatalysts are investigated by UV–Vis diffuse reflectance spectroscopy. As can be seen from Fig. 5a, compared to bare AgIO$_4$, the 7%GO–AgIO$_4$ nanocomposite shows much enhanced light absorption and a significant absorption-edge redshift, demonstrating that the introduction of GO into AgIO$_4$ can largely improve the light absorption of the AgIO$_4$ photocatalyst. Furthermore, the dynamics of separation and recombination of photoinduced electrons and holes of pure AgIO$_4$ and 7%GO–AgIO$_4$ nanocomposite was evaluated by PL spectroscopy. As shown in Fig. 5b, there are two main peaks at around 510 and 558 nm. Compared with those

of GO and pure AgIO$_4$, the intensities of the two peaks in the PL spectrum of 7%GO–AgIO$_4$ nanocomposite obviously decrease, indicating lower recombination rate of photoinduced electrons and holes. The result suggests that the photoinduced electrons of pure AgIO$_4$ could migrate to the GO nanosheets to reduce the subsequent electron–hole recombination [8]. In brief, after combining with GO, the charge separation of AgIO$_4$ can be effectively improved, which could favor the enhancement of photocatalytic activity.

Photocatalytic activity

The photocatalytic activities of the as-prepared GO–AgIO$_4$ nanocomposites were firstly evaluated by the
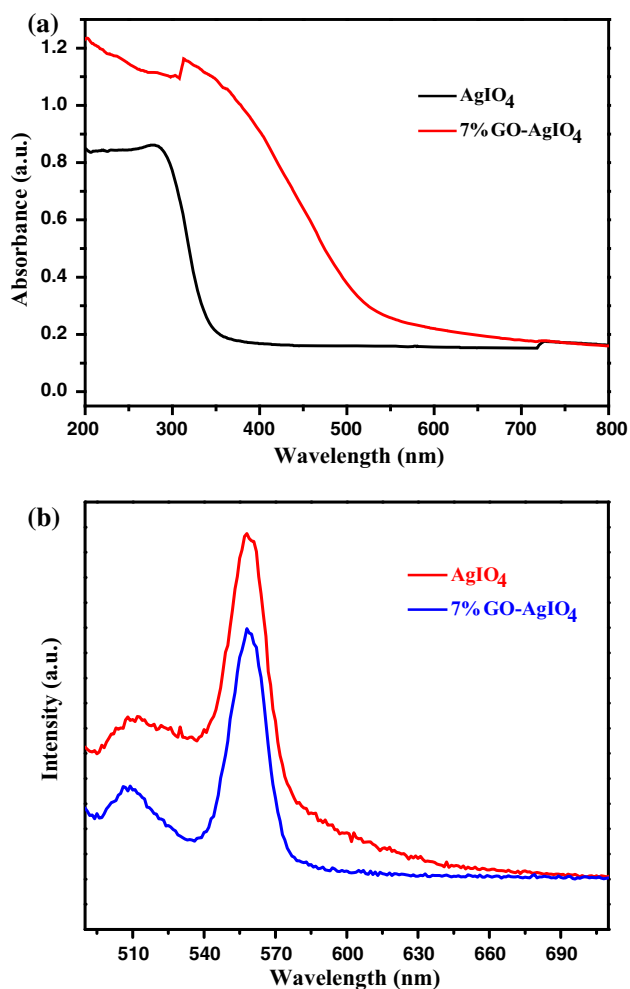
Figure 5 **a** UV–Vis diffuse reflectance spectra of the obtained pure AgIO$_4$ and 7%GO–AgIO$_4$ nanocomposite; **b** PL spectra of the obtained pure AgIO$_4$ and 7%GO–AgIO$_4$ with an excitation wavelength of 468 nm.

Figure 6 Photocatalytic degradation of MB by different photocatalysts under SSL irradiation.

degradation of MB under SSL irradiation at room temperature. As shown in Fig. 6, the blank test without any catalyst reveals that the self-photolysis of MB is negligible. The GO shows a poor photocatalytic activity. For pure AgIO$_4$ catalyst, the degradation ratio of MB reaches 89.14% after 40 min of irradiation. However, only 41.25% of MB could be degraded by AgIO$_4$ (Ref) within the same time. This suggests that a new AgIO$_4$ photocatalyst with better photocatalytic activity is developed as compared to the reported AgIO$_4$ (Ref) photocatalyst. The as-prepared GO–AgIO$_4$ nanocomposite catalysts can exhibit further enhanced photocatalytic activities compared to bare AgIO$_4$. With irradiation time of 40 min, the degradation ratios of 77.4, 97, and 94.7% can be achieved for 2%GO–AgIO$_4$, 7%GO–AgIO$_4$, and
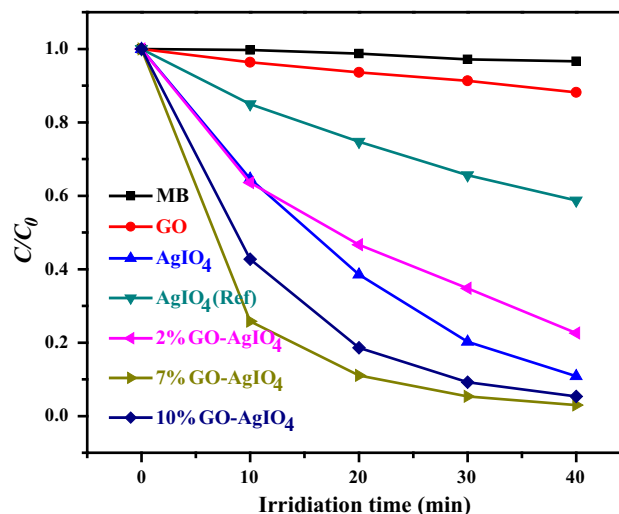
10%GO–AgIO$_4$, respectively. Therefore, the 7%GO–AgIO$_4$ nanocomposite displays the highest photocatalytic activity. The photocatalytic performance of 7%GO–AgIO$_4$ is also comparable to or even higher than that of previously reported GO-based photocatalysts such as GO/Ag@AgCl [31], GO/AgBr [23], GO/Ag/TiO$_2$ [40], and Ag$_3$PO$_4$/graphene [20]. The dramatically enhanced photocatalytic activities of the GO–AgIO$_4$ photocatalysts can be ascribed to the synergistic effect between GO and AgIO$_4$. It is because GO nanosheets could effectively promote the charge carriers separation and transfer, which plays an important role in improving the photocatalytic activity [41, 42]. However, introduction of an excessive amount of GO may lead to covering the active sites on the surface of AgIO$_4$, leading to a decrease in the photocatalytic activity, as evidenced by the 7%GO–AgIO$_4$ and 10%GO–AgIO$_4$ nanocomposites. Thus, the GO content has a significant influence on the photocatalytic activities of GO–AgIO$_4$ composite photocatalysts.

The stability of the 7%GO–AgIO$_4$ nanocomposite was investigated through the degradation of MB under the same condition for three successive cycles. The corresponding results are shown in Fig. 7a. After three recycling runs of the photodegradation of MB, the photocatalytic activity of 7%GO–AgIO$_4$ nanocomposite shows only a little loss, and the photocatalytic degradation efficiency is still as high as 90.5% after reacting for 40 min, indicating the GO–AgIO$_4$ nanocomposites possess good photocatalytic
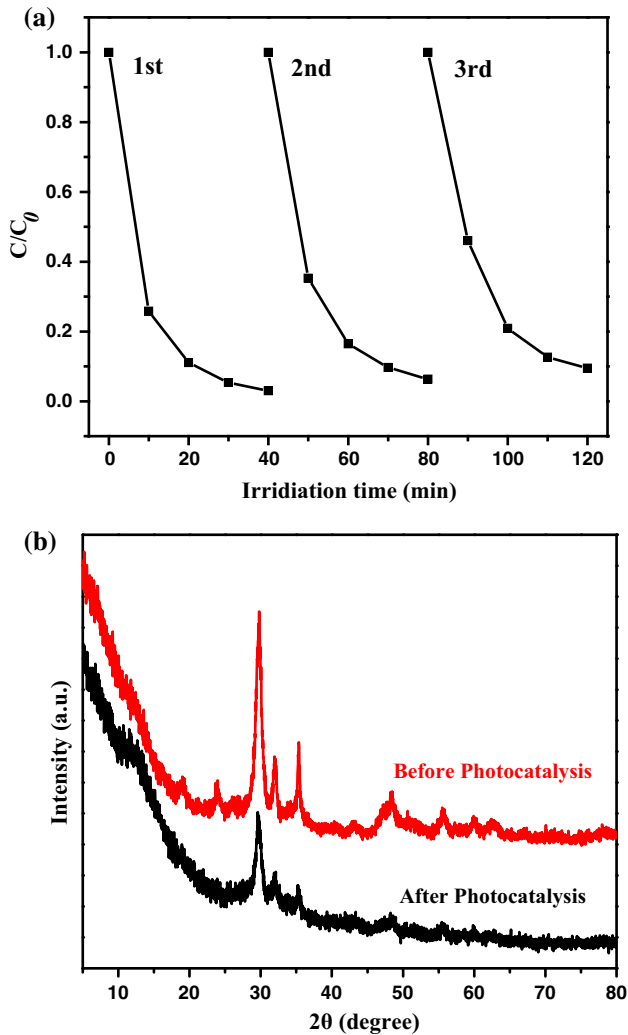
Figure 7 **a** The cycling runs of the photocatalytic degradation of MB with 7%GO–AgIO$_4$ photocatalyst; **b** XRD patterns of the 7%GO–AgIO$_4$ nanocomposite before and after three photocatalytic cycles.

Figure 8 Photocatalytic degradation of **a** RhB and **b** MO by pure AgIO$_4$, GO and 7%GO–AgIO$_4$ under SSL irradiation.

stability. As shown in Fig. 7b, the XRD pattern of the 7%GO–AgIO$_4$ nanocomposites before and after photocatalytic reaction also shows that the crystal structure of AgIO$_4$ has no obvious changes after the photocatalytic reaction. In addition, the structural stability of the photocatalysts after the catalytic reactions was also checked by TEM observation. As shown in Fig. S3, the morphology of the 7%GO–AgIO$_4$ photocatalyst does not display noticeable changes after catalysis. The mean size of AgIO$_4$ nanoparticles is 521 nm, which is consistent with the size before photocatalytic reaction. This further confirms the high stability of our prepared GO–AgIO$_4$ nanocomposite.
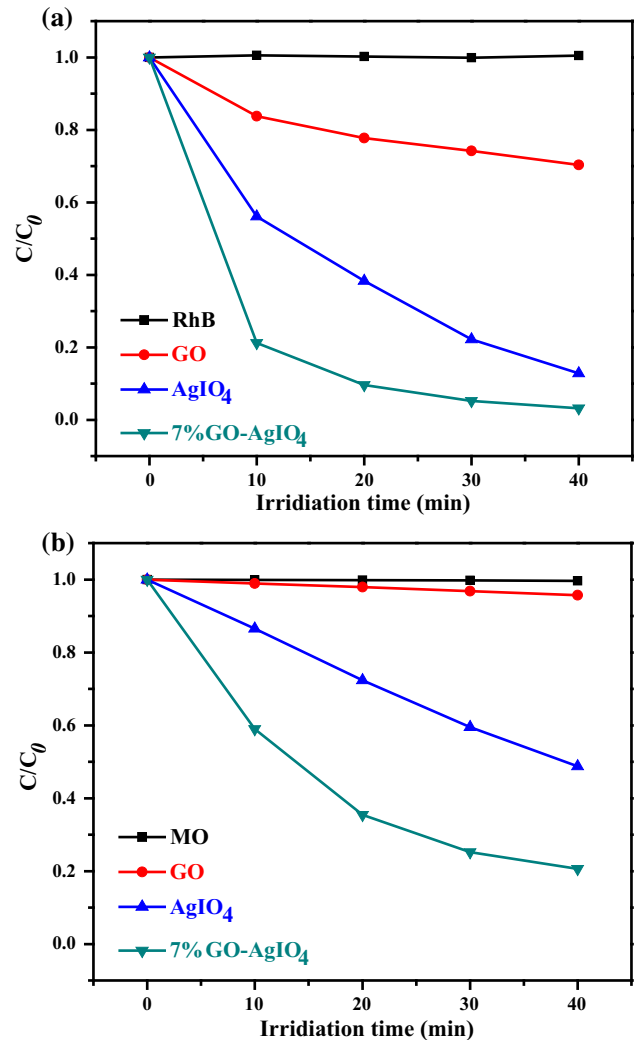
The photocatalytic performances of the as-synthesized samples were also studied for the degradation of RhB and MO, and the results are shown in Fig. 8a, b, respectively. The blank tests indicate that the self-photolysis of RhB and MO can be ignored. GO also shows poor photocatalytic activity in the degradation of RhB and MO. It can be seen from Fig. 8a that with 40 min irradiation, 96.8% of RhB is degraded by 7%GO–AgIO$_4$ catalyst, while for pure AgIO$_4$, the degradation efficiency is only 87.2%, demonstrating the enhanced catalytic performance of 7%GO–AgIO$_4$ for RhB degradation. A similar result is also found in the MO degradation. As shown in Fig. 8b, the photocatalytic activity of 7%GO–AgIO$_4$ (79.4%) is much higher than that of bare AgIO$_4$ (51.2%) in the MO degradation. It is worth noting that the GO–AgIO$_4$
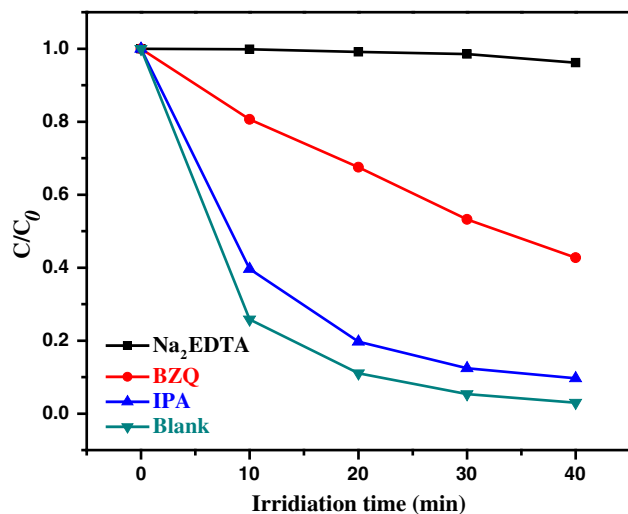
Figure 9 Photocatalytic degradation of MB by 7%GO–AgIO$_4$ nanocomposite in the presence of different scavengers under SSL irradiation.

catalyst shows much better photocatalytic performance for the degradation of cationic dyes (MB and RhB) than the anionic dye (MO), which is probably due to the negative surface of GO nanosheets, which can easily adsorb the cationic dyes by the electrostatic force and effectively promote the charge carriers separation and transfer [43]. Therefore, on the basis of the photocatalytic degradation results, it could be concluded that the introduction of GO efficiently improves the photocatalytic activity of the AgIO$_4$ photocatalyst. In addition, we also investigated the effect of the reduction degree of GO on the photocatalytic properties. As shown in Fig. S4, the AgIO$_4$ supported on GO shows a higher photocatalytic activity than that supported on pRGO and RGO. The reduced photocatalytic performance can be attributed to the inevitably reduction of AgIO$_4$ to Ag under the reduction process. The metal Ag on the surface of AgIO$_4$ nanoparticles could cause a light shielding effect to prevent AgIO$_4$ from absorbing light and also hinder the contact of MB molecules with AgIO$_4$, thus decreasing their photocatalytic efficiency. Moreover, because oxygen atoms have a larger electronegativity than carbon atoms, GO could become a p-type material. After reduction, RGO only behaves as an electron conductor and does not contribute to the generation of electrons and holes by the absorption of light [31]. Thus, the photocatalytic activities of the 7%pRGO–AgIO$_4$ and 7%RGO–AgIO$_4$ nanocomposites are relatively lower than that of 7%GO–AgIO$_4$.

Possible photocatalytic mechanism

As we known, organic dyes are photooxidized mainly by active species such as hydroxyl radicals (·OH), holes (h$^+$) and superoxide radicals (O$_2^{·-}$) [44]. To understand the photocatalytic reaction mechanism, we employed isopropanol (IPA), disodium ethylenediaminetetraacetate (Na$_2$EDTA), and p-benzoquinone (BZQ) acting as ·OH, h$^+$ and O$_2^{·-}$ scavenger, respectively, in separate experiments. The results are shown in Fig. 9. It can be seen that when 10 mM IPA was added into MB solution, there is little effect on the photocatalytic activity of the GO–AgIO$_4$ catalyst, while the addition of 1 mM of BZQ or 1 mM of Na$_2$EDTA results in the fast deactivation of the catalyst. In particular, Na$_2$EDTA can almost completely deactivate the catalytic process. The above results mean that h$^+$ and O$_2^{·-}$ contribute mostly to the photocatalytic process of the GO–AgIO$_4$ nanocomposites.

Based on the above analysis, we propose the possible photocatalytic mechanism. As shown in Fig. 10, under light irradiation, the electrons (e$^-$) at the valence band (VB) of AgIO$_4$ are excited to the conduction band (CB), causing the formation of holes (h$^+$) in the VB. Then, the electrons can reduce O$_2$ into O$_2^{·-}$ as the active species [45]; meanwhile, the holes can directly oxidize organic dyes. However, when AgIO$_4$ particles are dispersed on the surface of GO nanosheets, these electrons on the CB of AgIO$_4$ tend to transfer to GO nanosheets, leading to the hole–electron pairs to be separated more efficiently [35]. Thus, more electrons and holes can be utilized in the photodegradation process and the photocatalytic activity is improved.
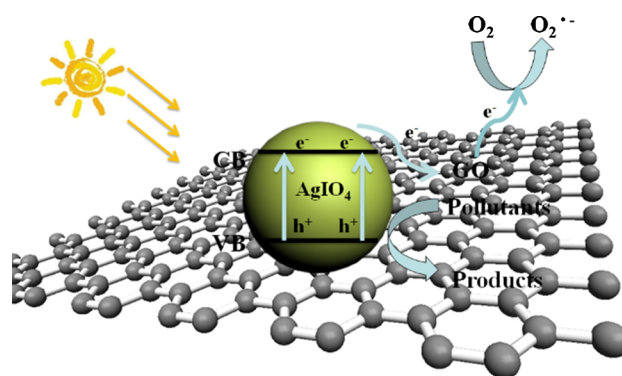

Figure 10 Proposed photocatalytic mechanism for GO–AgIO$_4$ nanocomposites under SSL irradiation.

Conclusion

In summary, a facile ion-exchange method has been developed for the synthesis of GO–AgIO$_4$ composites. The GO–AgIO$_4$ composites exhibit a significantly enhanced photocatalytic activity in the degradation of organic pollutants under SSL irradiation compared to the bare AgIO$_4$. It is revealed that the content of GO has a significant influence on the photocatalytic performance of the GO–AgIO$_4$ composites. The introduction of GO nanosheets could decrease the particle size of AgIO$_4$, increase light absorption, and promote the effective separation of photoexcited electron–hole pairs. The graphene-based AgIO$_4$ photocatalysts with excellent photocatalytic activity promise potential application in organic pollutant treatment.

Acknowledgements

Electronic supplementary material: The online version of this article (doi:10.1007/s10853-017-0849-4) contains supplementary material, which is available to authorized users.

References

[1] Karthikeyan S, Boopathy R, Sekaran G (2015) In situ generation of hydroxyl radical by cobalt oxide supported porous carbon enhance removal of refractory organics in tannery dyeing wastewater. J Colloid Interface Sci 448:163–174

[2] Pachamuthu MP, Karthikeyan S, Maheswari R, Lee AF, Ramanathan A (2017) Fenton-like degradation of Bisphenol A catalyzed by mesoporous Cu/TUD-1. Appl Surf Sci 393:67–73

[3] Karthikeyan S, Dionysiou DD, Lee AF, Suvitha S, Maharaja P, Wilson K, Sekaran G (2016) Hydroxyl radical generation by cactus like copper oxide nanoporous carbon catalysts for microcystin-LR environmental remediation. Catal Sci Technol 6:530–544

[4] Jo WK, Kumar S, Isaacs MA, Lee AF, Karthikeyan S (2017) Cobalt promoted TiO$_2$/GO for the photocatalytic degradation of oxytetracycline and Congo Red. Appl Catal B 201:159–168

[5] Tong H, Ouyang SX, Bi YP, Umezawa N, Oshikiri M, Ye JH (2012) Nano-photocatalytic materials: possibilities and challenges. Adv Mater 24:229–251

[6] Xie XQ, Kretschmer K, Wang GX (2015) Advances in graphene-based semiconductor photocatalysts for solar energy conversion: fundamentals and materials engineering. Nanoscale 7:13278–13292

[7] Cui XF, Jiang GY, Zhao Z, Xu CM, Bai WK, Wang YJ, Duan AJ, Liu J, Wei YC (2016) Facile regulation of crystalline phases and exposed facets on Ti^{3+} self-doped TiO$_2$ for efficient photocatalytic hydrogen evolution. J Mater Sci 51:10819–10832. doi:10.1007/s10853-016-0293-x

[8] Song SQ, Cheng B, Wu NS, Meng AY, Cao SW, Yu JG (2016) Structure effect of graphene on the photocatalytic performance of plasmonic Ag/Ag$_2$CO$_3$–rGO for photocatalytic elimination of pollutants. Appl Catal B 181:71–78

[9] Zhang M, Bai XJ, Liu D, Wang J, Zhu XF (2015) Enhanced catalytic activity of potassium-doped graphitic carbon nitride induced by lower valence position. Appl Catal B 164:77–81

[10] Zhang H, Guo LH, Wang DB, Zhao LX, Wan B (2015) Light-induced efficient molecular oxygen activation on a Cu(II)-Grafted TiO$_2$/graphene photocatalyst for phenol degradation. ACS Appl Mater Interfaces 7:1816–1823

[11] Wu ZY, Zhao GH, Zhang YJ, Liu J, Zhang YN, Shi HJ (2015) A solar-driven photocatalytic fuel cell with dual photoelectrode for simultaneous wastewater treatment and hydrogen production. J Mater Chem A 3:3416–3424

[12] Leblebici ME, Ronge J, Martens JA, Stefanidis GD, Van Gerven T (2015) Computational modelling of a photocatalytic UV-LED reactor with internal mass and photon transfer consideration. Chem Eng J 264:962–970

[13] Liu J, Liu Y, Liu NY, Han YZ, Zhang X, Huang H, Kang ZH (2015) Metal-free efficient photocatalyst for stable visible water splitting via a two-electron pathway. Science 347:970–974

[14] Xiang QJ, Yu JG, Jaroniec M (2012) Synergetic effect of MoS$_2$ and graphene as cocatalysts for enhanced photocatalytic H$_2$ production activity of TiO$_2$ nanoparticles. J Am Chem Soc 134:6575–6578

[15] Park S, Ruoff RS (2009) Chemical methods for the production of graphenes. Nat Nanotechnol 4:217–224

[16] Jang BZ, Liu VG, Neff D, Yu ZN, Wang MC, Xiong W, Zhamu A (2011) Graphene surface-enabled lithium ion-

exchanging cells: next-generation high-power energy storage devices. Nano Lett 11:3785–3791

[17] Dong C, Wu KL, Wei XW, Li XZ, Liu L, Ding TH, Ye Y (2014) Synthesis of graphene oxide-Ag_2CO_3 composites with improved photoactivity and antiphotocorrosion. CrystEngComm 16:730–736

[18] Wang WG, Yu JG, Xiang QJ, Cheng B (2012) Enhanced photocatalytic activity of hierarchical macro/mesoporous TiO_2–graphene composites for photodegradation of acetone in air. Appl Catal B 119:109–116

[19] Yang XF, Cui HY, Li Y, Qin JL, Zhang RX, Tang H (2013) Fabrication of Ag_3PO_4–graphene composites with highly efficient and stable visible light photocatalytic performance. ACS Catal 3:363–369

[20] Chen GD, Sun M, Wei Q, Zhang YF, Zhu BC, Du B (2013) Ag_3PO_4/graphene-oxide composite with remarkably enhanced visible-light-driven photocatalytic activity toward dyes in water. J Hazard Mater 244:86–93

[21] Xu L, Huang WQ, Wang LL, Huang GF, Peng P (2014) Mechanism of superior visible-light photocatalytic activity and stability of hybrid Ag_3PO_4/graphene nanocomposite. J Phys Chem C 118:12972–12979

[22] Esmaeili A, Entezari MH (2015) Cubic Ag/AgBr–graphene oxide nanocomposite: sono-synthesis and use as a solar photocatalyst for the degradation of DCF as a pharmaceutical pollutant. RSC Adv 5:97027–97035

[23] Zhang D, Tang H, Wang YQ, Wu KQ, Huang H, Tang GG, Yang J (2014) Synthesis and characterization of graphene oxide modified AgBr nanocomposites with enhanced photocatalytic activity and stability under visible light. Appl Surf Sci 319:306–311

[24] Fan YY, Ma WG, Han DX, Gan SY, Dong XD, Niu L (2015) Convenient recycling of 3D AgX/graphene aerogels (X = Br, Cl) for efficient photocatalytic degradation of water pollutants. Adv Mater 27:3767–3773

[25] Luo GQ, Jiang XJ, Li MJ, Shen Q, Zhang LM, Yu HG (2013) Facile fabrication and enhanced photocatalytic performance of Ag/AgCl/rGO heterostructure photocatalyst. ACS Appl Mater Interfaces 5:2161–2168

[26] Wang YQ, Fugetsu B (2013) A polyelectrolyte-stabilized approach for massive production of AgCl/graphene nanocomposites. Chem Lett 42:438–440

[27] Tang JT, Li DT, Feng ZX, Tan Z, Ou BL (2014) A novel $AgIO_4$ semiconductor with ultrahigh activity in photodegradation of organic dyes: insights into the photosensitization mechanism. RSC Adv 4:2151–2154

[28] Hummers WS, Offeman RE (1958) Preparation of graphitic oxide. J Am Chem Soc 80:1339

[29] Ji ZY, Shen XP, Zhu GX, Zhou H, Yuan AH (2012) Reduced graphene oxide/nickel nanocomposites: facile synthesis,

magnetic and catalytic properties. J Mater Chem 22:3471–3477

[30] Qin JW, Cao MH, Li N, Hu CW (2011) Graphene-wrapped WO_3 nanoparticles with improved performances in electrical conductivity and gas sensing properties. J Mater Chem 21:17167–17174

[31] Min YL, He GQ, Xu QJ, Chen YC (2014) Self-assembled encapsulation of graphene oxide/Ag@AgCl as a Z-scheme photocatalytic system for pollutant removal. J Mater Chem A 2:1294–1301

[32] Park S, An J, Potts JR, Velamakanni A, Murali S, Ruoff RS (2011) Hydrazine-reduction of graphite and graphene oxide. Carbon 49:3019–3023

[33] Dai K, Lu LH, Liang CH, Dai JM, Liu QZ, Zhang YX, Liu ZL (2014) In situ assembly of MnO_2 nanowires/graphene oxide nanosheets composite with high specific capacitance. Electrochim Acta 116:111–117

[34] Qiu L, Yang X, Gou X, Yang W, Ma ZF, Wallace GG, Li D (2010) Dispersing carbon nanotubes with graphene oxide in water and synergistic effects between graphene derivatives. Chem Eur J 16:10653–10658

[35] Pasricha R, Gupta S, Srivastava AK (2009) Facile, novel synthesis of Ag–graphene-based nanocomposites. Small 5:2253–2259

[36] Ji ZY, Shen XP, Yang JL, Zhu GX, Chen KM (2014) A novel reduced graphene oxide/Ag/CeO_2 ternary nanocomposite: green synthesis and catalytic properties. Appl Catal B 144:454–461

[37] Shah MSS, Zhang K, Park AR, Kim KS, Park NG, Park JH, Yoo PJ (2013) Single-step solvothermal synthesis of mesoporous Ag–TiO_2-reduced graphene oxide ternary composites with enhanced photocatalytic activity. Nanoscale 5:5093–5101

[38] Nethravathi C, Rajamathi M (2008) Chemically modified graphene sheets produced by the solvothermal reduction of colloidal dispersions of graphite oxide. Carbon 46:1994–1998

[39] Wang C, Zhu JX, Wu XY, Xu H, Song YH, Yan J, Song YX, Ji HY, Wang K, Li HM (2014) Photocatalytic degradation of bisphenol A and dye by graphene-oxide/Ag_3PO_4 composite under visible light irradiation. Ceram Int 40:8061–8070

[40] Sim LC, Leong KH, Ibrahim S, Saravanan P (2014) Graphene oxide and Ag engulfed TiO_2 nanotube arrays for enhanced electron mobility and visible light-driven photocatalytic performance. J Mater Chem A 2:5315–5322

[41] Liu L, Liu JC, Sun DD (2012) Graphene oxide enwrapped Ag_3PO_4 composite: towards a highly efficient and stable visible-light-induced photocatalyst for water purification. Catal Sci Technol 2:2525–2532

[42] Liu J, Bai H, Wang Y, Liu Z, Zhang X, Sun DD (2010) Self-assembling TiO$_2$ nanorods on large graphene oxide sheets at a two-phase interface and their anti-recombination in photocatalytic applications. Adv Funct Mater 20:4175–4181

[43] Oh J, Lee S, Zhang K, Hwang JO, Han J, Park G, Kim SO, Park JH, Park S (2014) Graphene oxide-assisted production of carbon nitrides using a solution process and their photocatalytic activity. Carbon 66:119–125

[44] Li WJ, Li DZ, Lin YM, Wang PX, Chen W, Fu XZ, Shao Y (2012) Evidence for the active species involved in the photodegradation process of methyl orange on TiO$_2$. J Phys Chem C 116:3552–3560

[45] Yu JG, Dai GP, Huang BB (2009) Fabrication and characterization of visible-light-driven plasmonic photocatalyst Ag/AgCl/TiO$_2$ nanotube arrays. J Phys Chem C 113:16394–16401